Electronic Supplementary Information

Redox-triggered reversible modulation of intense near-infrared and visible absorption using paddlewheel-type diruthenium(III) complex

Yusuke Kataoka,*[a], Nanako Imasaki,[a] Natsumi Yano,[b] Minoru Mitsumi,[c] Makoto Handa[a]

[a] Department of Chemistry, Graduate School of Natural Science and Technology, Shimane University.
[b] Special Course in Science and Engineering, Graduate School of Natural Science and Technology, Shimane University.
[c] Department of Chemistry, Faculty of Science, Okayama University of Science.

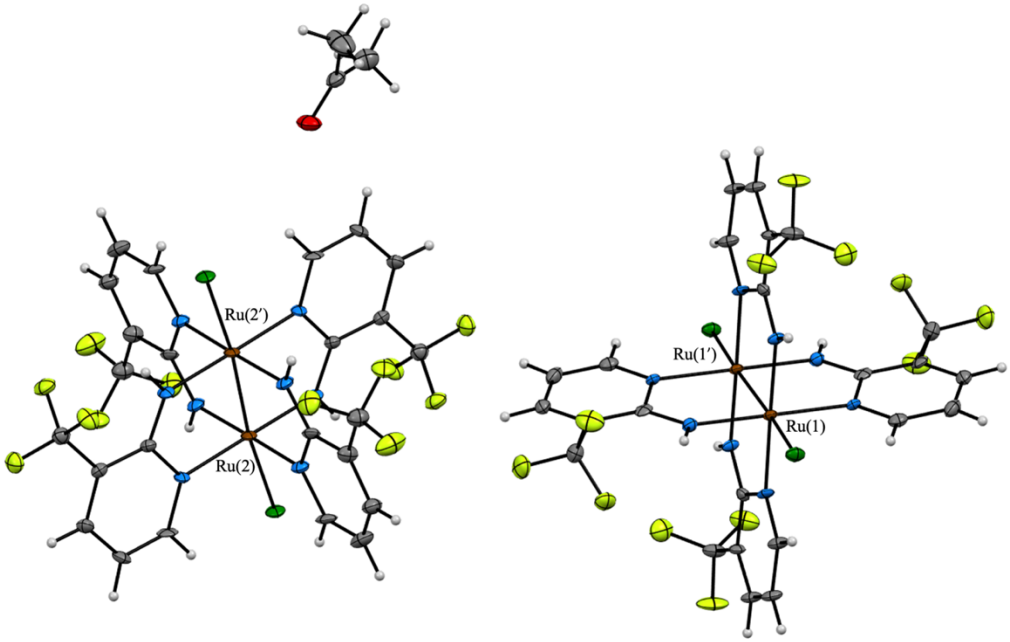

Fig. S1 Full crystal structure of [1] with thermal ellipsoids at a 30% probability (Ru: brown, Cl: green, F: yellow, O: red, N: blue, C: gray, H: white).

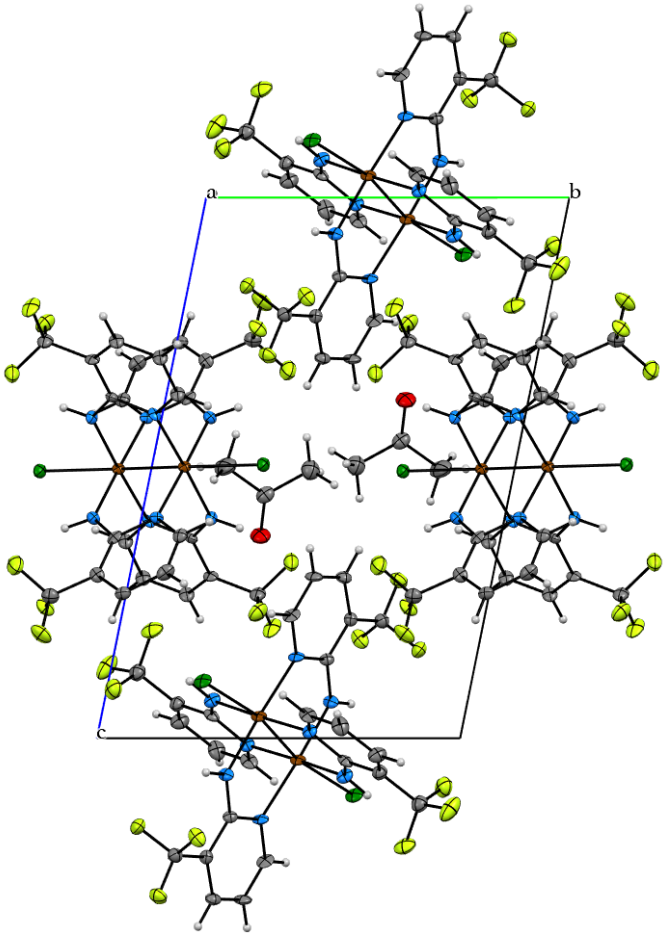

Fig. S2 Packing view of [1] along a-axis (thermal ellipsoids at a 30% probability; Ru: brown, Cl: green, F: yellow, O: red, N: blue, C: gray, H: white).

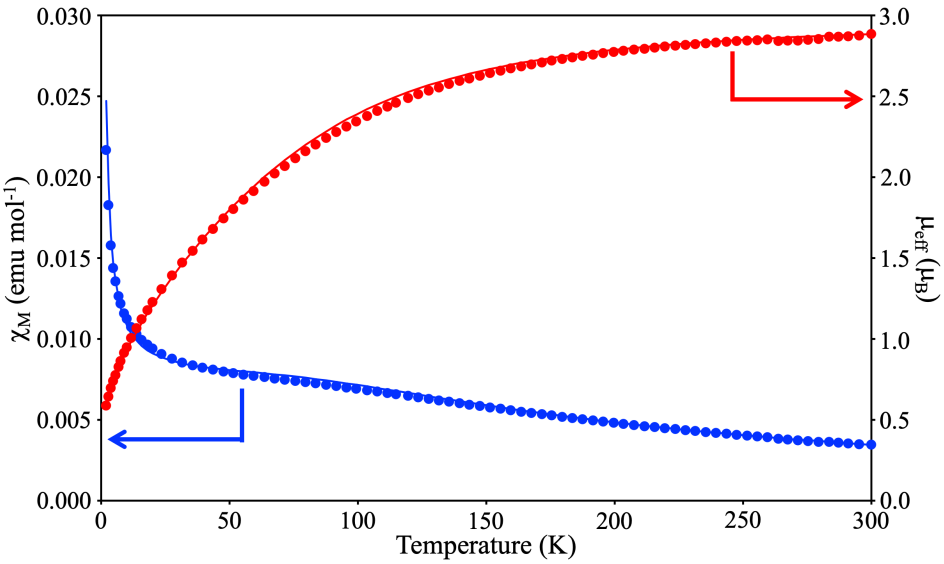

Fig. S3 Temperature dependence of magnetic susceptibility (blue dots) and effective magnetic moments (red dots) of [1]. The solid lines are drawn with the simulated values of $g = 2.08$, $D = 200$ cm^{-1}, and ρ (for paramagnetic impurity with S = 3/2 (Ru_2^{5+}) species). The details of the simulation are described elsewhere [ref. S2]

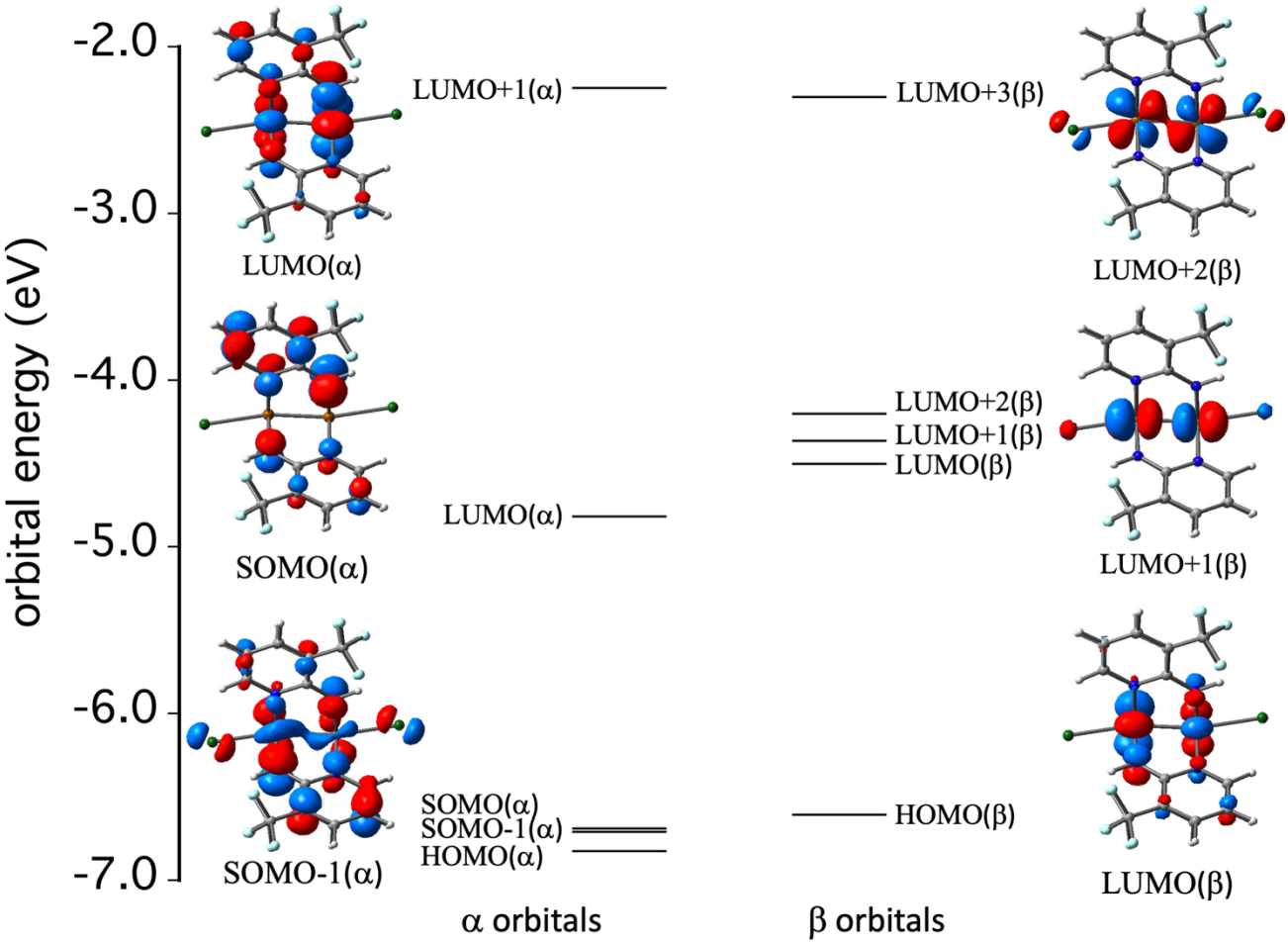

Fig. S4 Molecular orbitals of [1]. Here, the HOMO, LUMO, and SOMO are highest-occupied MO, lowest unoccupied MO, and singly occupied MO, respectively.

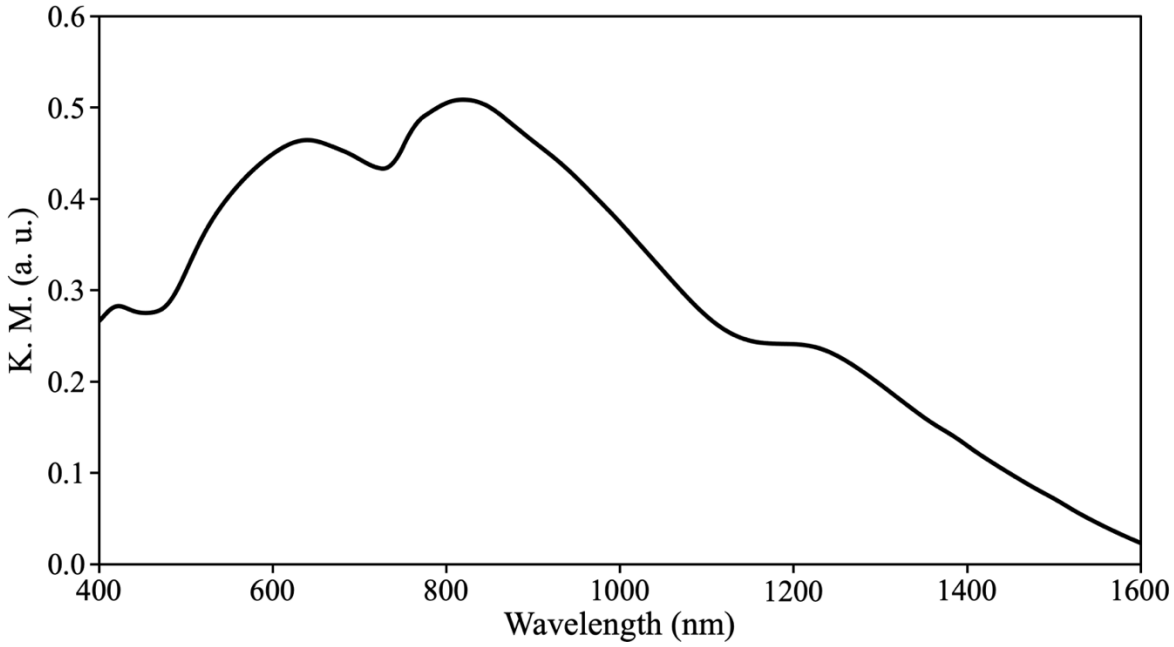

Fig. S5 Solid-state diffuse reflectance spectrum of [1].

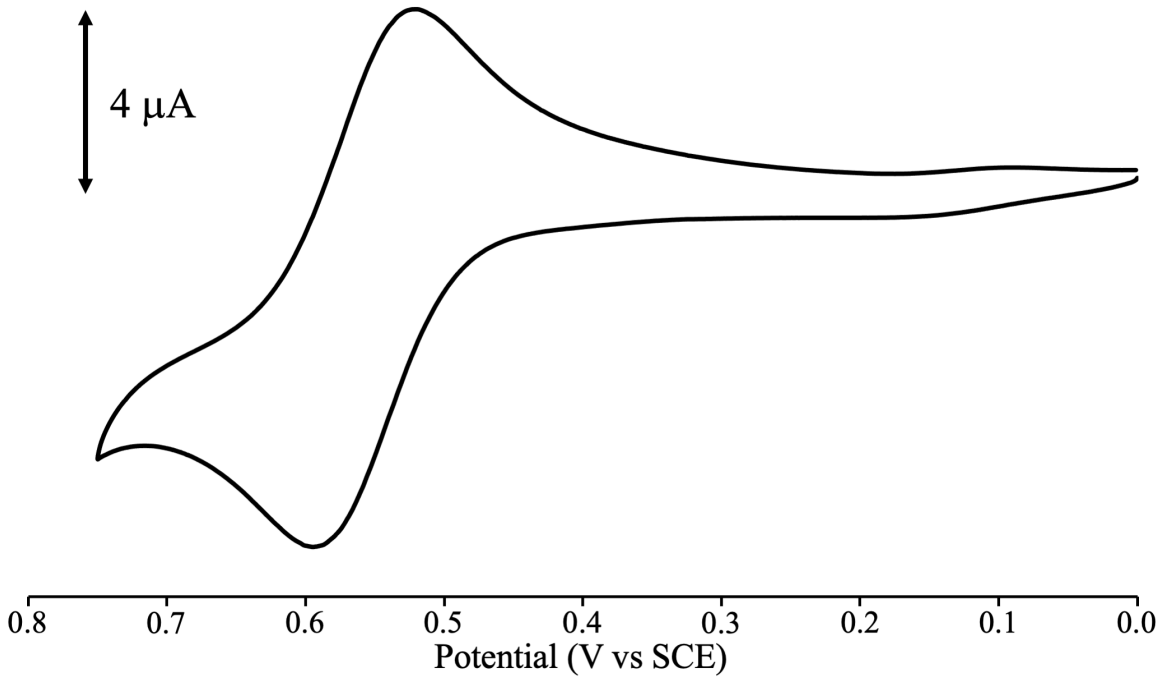

Fig. S6 CV measurement of [1] (1.0 mM) in DMF with 0.10 M [*n*-Bu_4N]Cl (scan rate: 50 mVs^{-1}).

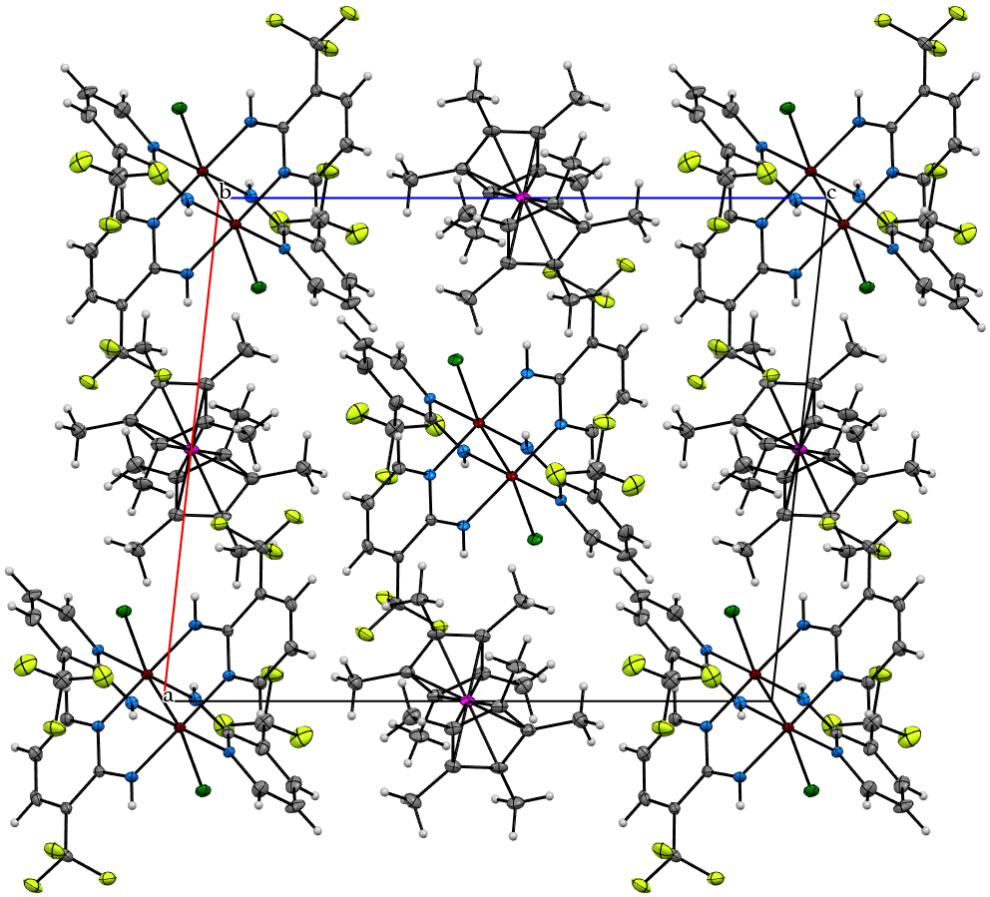

Fig. S7 Packing view of [CoCp*$_2$][1] along b-axis (thermal ellipsoids at a 20% probability; Ru: brown, Cl: green, F: yellow, O: red, N: blue, C: gray, H: white).

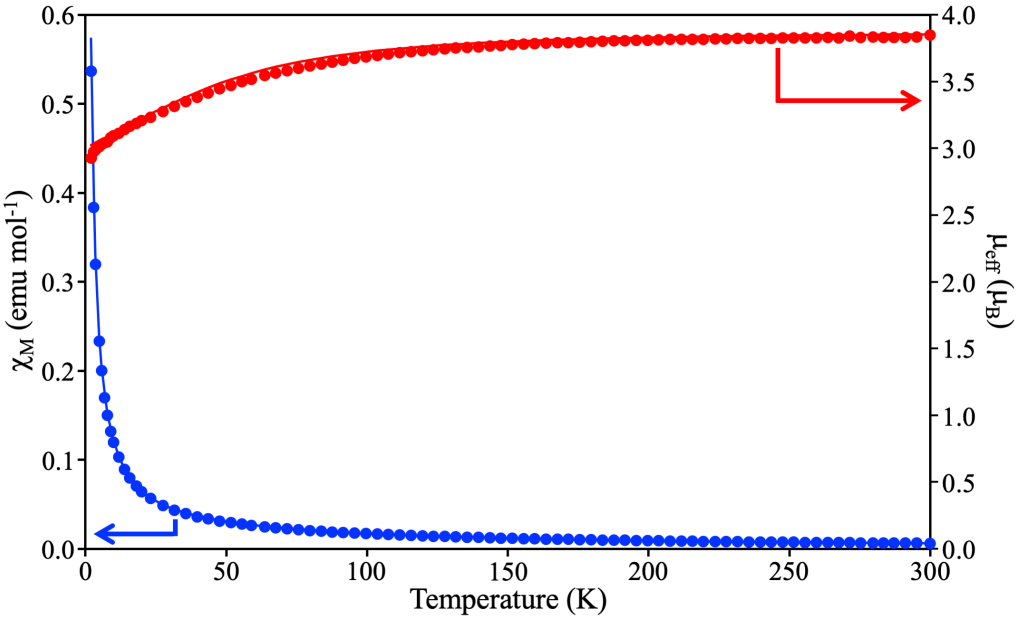

Fig. S8 Temperature dependence of magnetic suscep tibility (blue dots) and effective magnetic moments (red dots) of [CoCp*$_2$][1]. The solid lines are drawn with the simulated values of g = 2.00 and D = 60 cm^{-1}. The details of the simulation are described elsewhere [ref. S3].

Table S1. Crystallographic data of [1] and [CoCp*$_2$][1].

	[1]	[CoCp*$_2$][1]
Formula	$C_{27}H_{22}Cl_2F_{12}N_8ORu_2$	$C_{44}H_{46}Cl_2CoF_{12}N_8Ru_2$
M_r (g mol^{-1})	975.56	1246.86
Crystal system	triclinic	monoclinic
Space group	*P*-1	*P* 2$_1$/*n*
a (Å)	10.661(5)	14.0204(5)
b (Å)	11.254(6)	10.3722(4)
c (Å)	15.836(7)	16.8406(6)
α (deg)	100.225(5)	90
β (deg)	90.827(6)	96.297(3)
γ (deg)	112.350(6)	90
V (Å^3)	1722.3(14)	2434.22(16)
Z	2	2
D_{calc} (g cm^{-3})	1.881	1.701
μ (mm^{-1})	1.134	1.147
F(000)	956	1246
R_1 ($I > 2\sigma(I)$)	0.0605	0.0799
wR_2 ($I > 2\sigma(I)$)	0.1380	0.1883
R_1 (all data)	0.0788	0.0840
wR_2 (all data)	0.1574	0.1898
GOF on F^2	0.973	1.358

Table S2. Selected structural parameters (length: Å, angle: º) of crystal structure of [1].

Bond lengths (Å)			
Ru(1)-Ru(1′)	2.3296(15)	Ru(2)-N(2′)	2.3307(12)
Ru(1)-Cl(1)	2.510(2)	Ru(2)-Cl(2)	2.5186(19)
Ru(1)-N(1′)	2.094(5)	Ru(2)-N(5′)	2.066(6)
Ru(1)-N(2)	2.011(5)	Ru(2)-N(6)	1.973(6)
Ru(1)-N(3′)	2.081(6)	Ru(2)-N(7′)	2.069(6)
Ru(1)-N(4)	1.995(6)	Ru(2)-N(8)	2.007(6)
C(1)-N(1)	1.375(8)	C(13)-N(5)	1.381(9)
C(1)-N(2)	1.301(8)	C(13)-N(6)	1.338(8)
C(7)-N(3)	1.374(9)	C(19)-N(7)	1.371(9)
C(7)-N(4)	1.327(9)	C(19)-N(8)	1.337(8)
Bond angle (°)			
Ru(1′)-Ru(1)-Cl(1)	170.44(5)	Ru(2′)-Ru(2)-Cl(2)	167.81(6)
N(1′)-Ru(1)-Ru(1′)	90.62(14)	N(5′)-Ru(2)-Ru(2′)	92.38(14)
N(2)-Ru(1)-Ru(1′)	88.04(15)	N(6)-Ru(2)-Ru(2′)	86.38(15)
N(3′)-Ru(1)-Ru(1′)	90.85(14)	N(7′)-Ru(2)-Ru(2′)	91.26(15)
N(4)-Ru(1)-Ru(1′)	87.83(16)	N(8)-Ru(2)-Ru(2′)	87.27(15)
N(1′)-Ru(1)-N(3′)	90.5(2)	N(5′)-Ru(2)-N(7′)	87.5(2)
N(1′)-Ru(1)-N(4)	88.9(2)	N(5′)-Ru(2)-N(8)	90.1(3)
N(2)-Ru(1)-N(4)	92.5(2)	N(6)-Ru(2)-N(8)	92.4(3)
N(2)-Ru(1)-N(3′)	88.0(2)	N(6)-Ru(2)-N(7′)	89.9(3)

Table S3. Result of TDDFT calculation of [1]. Here, H, L, and S are HOMO, LUMO, and SOMO, respectively.

Wavelength (nm)	Oscillator Strength	Excitation characters	Observed absorption bands (nm)
1301.8	0.0068	S(α)[π(amtfmp)] → L(α)[δ*(Ru_2)] (67%) H-1(β)[π(amtfmp)] → L(β)[δ*(Ru_2)] (24%)	1350-1160
998.3	0.0067	H-1(α)[π(amtfmp)] → L(α)[δ*(Ru_2)] (58%) H-2(β)[π(amtfmp)] → L(β)[δ*(Ru_2)] (19%) H-1(β)[π(amtfmp)] → L(β)[δ*(Ru_2)] (11%)	880
987.8	0.0123	H-4(β)[π(Ru_2)] → L+1(β)[π*(Ru_2)] (31%), H(β)[δ(Ru_2)/π(amtfmp)] → L(β)[δ*(Ru_2)] (19%), H-3(β)[σ(Ru_2)] → L+1(β)[π*(Ru_2)] (13%), H-1(β)[π(amtfmp)] → L+1(β)[π*(Ru_2)] (15%) H-1(α)[π(amtfmp)] → L(α)[δ*(Ru_2)] (9%)	
923.7	0.0066	H-3(α)[σ(Ru_2)] → L(α)[δ*(Ru_2)] (31%) H-3(β)[σ(Ru_2)] → L(β)[δ*(Ru_2)] (41%) H(β)[δ(Ru_2)/π(amtfmp)] → L(β)[δ*(Ru_2)] (9%)	
900.2	0.0139	H-3(β)[σ(Ru_2)] → L+2(β)[π*(Ru_2)] (24%) H-3(α)[σ(Ru_2)] → L(α)[δ*(Ru_2)] (23%), S-1(α)[d(Ru_2)/π(amtfmp)] → L(α)[δ*(Ru_2)] (12%), H-5(β)[π(Ru_2)] → L+2(β)[π*(Ru_2)] (10%), H-1(β)[π(amtfmp)] → L+1(β)[π*(Ru_2)] (10%), H(β)[δ(Ru_2)/π(amtfmp)] → L(β)[δ*(Ru_2)] (12%)	
863.8	0.0023	H-3(β)[σ(Ru_2)] → L+2(β)[π*(Ru_2)] (68%) H-1(β)[d(Ru_2)/π(amtfmp)] → L+1(β)[π*(Ru_2)] (15%)	
630.3	0.1402	H-2(β)[π(amtfmp)]→L(β)[δ*(Ru_2)] (70%) , S-1(α)[d(Ru_2)/π(amtfmp)] → L(α)[δ*(Ru_2)] (20%)	672
622.8	0.0079	H-2(β)[π(amtfmp)] → L+2(β)[π*(Ru_2)] (70%)	

Table S4. Selected structural parameters (length: Å, angle: º) of crystal structure of [$CoCp^*_2$][1].

Bond lengths (Å)			
Ru(1)-Ru(1′)	2.3066(16)	Ru(1)-Cl(1)	2.539(3)
Ru(1)-N(1′)	2.091(8)	C(1)-N(1)	1.375(12)
Ru(1)-N(2)	2.025(8)	C(1)-N(2)	1.313(13)
Ru(1)-N(3′)	2.076(9)	C(7)-N(3)	1.372(14)
Ru(1)-N(4)	2.031(8)	C(7)-N(4)	1.320(13)
Bond angle (°)			
Ru(1′)-Ru(1)-Cl(1)	171.38(8)	N(1′)-Ru(1)-N(3′)	90.8(3)
N(1′)-Ru(1)-Ru(1′)	91.6(2)	N(1′)-Ru(1)-N(4)	88.8(3)
N(2)-Ru(1)-Ru(1′)	87.6(2)	N(2)-Ru(1)-N(4)	90.6(3)
N(3′)-Ru(1)-Ru(1′)	90.9(2)	N(2)-Ru(1)-N(3′)	89.8(3)
N(4)-Ru(1)-Ru(1′)	88.5(2)		